ELSEVIER

Journal of Marine Systems 21 (1999) 55–65

JOURNAL OF MARINE SYSTEMS

Parameterization of mixing in the ocean boundary layer

Miles G. McPhee *

McPhee Research, 450 Springs Road, Naches, WA 98937, USA

Received 14 November 1997; accepted 9 July 1998

Abstract

A method for estimating eddy viscosity and diffusivity based on a similarity theory for the vertical exchange scale of dominant turbulent eddies in a surface forced flow is used to predict flux profiles for momentum, heat, and salt in the ocean boundary layer (OBL). By neglecting time dependence in solving for the turbulence properties, the technique requires specifying only the mean density profile along with surface friction velocity and surface buoyancy flux. Momentum and scalar fluxes in stratified fluid below the well-mixed layer are determined by iteration. The method is illustrated in two ways. First, measurements of turbulent stress and heat flux from an intense storm during the 1994 Antarctic Zone Flux Experiment are simulated with reasonable accuracy. The model is forced by Reynolds stress measured near the surface, and by buoyancy flux estimated from the thermodynamic mass balance at the ice undersurface. It is then verified by comparing predicted friction velocity with measurements at other levels in the boundary layer, and by comparing predicted and measured turbulent heat flux. The latter requires accurate simulation of eddy diffusivity in the boundary layer. In the second demonstration, a prognostic model for the evolution of upper ocean temperature and salinity structure is formulated for an idealized storm scenario in which freezing or melting at the surface alternately induces destabilizing and stabilizing surface buoyancy flux. Since closure is local, prognostic equations for temperature and salinity only are carried. The model simulations are compared with a second-moment closure model (Mellor–Yamada level $2\frac{1}{2}$) forced in the same way. For surface heat flux (the main diagnostic), the two approaches agree quite well. In other respects, significant differences are noted, and it is suggested how data may be used to evaluate (and discriminate among) ocean turbulence models.

Keywords: parameterization; mixing; ocean

1. Introduction

Specification of the 'mixing length' applicable to first-order or higher-order turbulence closure models remains a fundamental issue in numerical modeling of ocean boundary layers (OBLs). Here, an algorithm based on mean quantity and flux measurements in the OBL that develops under drifting sea ice (McPhee, 1994) is combined with a turbulent friction velocity to specify eddy viscosity and diffusivity in both the mixed layer and in the actively mixing upper pycnocline. The method assumes that boundary layer turbulence adjusts rapidly to changes in surface flux conditions, and that a good approximation of the turbulent structure of the boundary may be obtained based only on instantaneous surface

* Tel.: +1-509-658-2575; Fax: +1-509-658-2575; E-mail: miles@wolfenet.com, miles@apl.washington.edu

0924-7963/99/$ - see front matter
PII: S0924-7963(99)00005-6

stress and buoyancy flux, and the existing mean temperature and salinity (T/S) profiles. Advection of turbulent kinetic energy is neglected, thus, the closure depends only on local forcing, and is referred to as local turbulence closure (LTC).

Unlike bulk or slab-mixed layer models (e.g., Price et al., 1986), the LTC approach considers mean quantity gradients and finite (but variable) eddy viscosity and diffusivity in the mixed layer and underlying pycnocline. This is required for consistency with numerous observations from the OBL under drifting sea ice that show detectable (albeit small) gradients whenever fluxes are measured (McPhee, 1992, 1994; McPhee and Martinson, 1994; McPhee and Stanton, 1996). The method differs from turbulence models derived from second-moment closure of the Navier–Stokes equations (e.g., Mellor and Yamada, 1982 level $2\frac{1}{2}$ or $k-\varepsilon$; Burchard and Baumert, 1995) by prescribing the dominant turbulence scales in two distinct regions of the flow: (i) in a *mixing layer* above the pycnocline where property gradients are relatively small, and the scale is determined by turbulent stress and buoyancy flux at the surface; and (ii) in the upper pycnocline, where gradients are large and the scale is determined by stress and buoyancy flux at the interface between the mixing layer and the pycnocline.

In this paper, LTC is applied in two ways. It is used first as an iterative technique for combining profiles of temperature and salinity with turbulent stress measured at one level in the boundary layer to describe the remainder of the boundary layer in considerable detail. Unlike the atmospheric surface layer where an extensive set of formulas exists for relating boundary layer measurements to surface flux conditions (Monin–Obukhov similarity theory, e.g., Businger et al., 1971), there is no generally accepted method for extending turbulence measurements made at one or more levels in the outer part of the boundary layer to other levels, and to the surface.

In the second application a prognostic model is solved for the evolution of the temperature, salinity and surface fluxes of heat and salt for an idealized scenario of extreme forcing meant to mimic aspects of turbulent oceanic heat exchange in the Weddell Sea in winter. The model uses expressions for eddy viscosity and scalar diffusivity based on local conditions only. Results are compared with a more conventional, Mellor–Yamada level $2\frac{1}{2}$ closure (Mellor and Yamada, 1982) turbulence model.

The method described here is much like the similarity turbulence closure model suggested in previous work (McPhee, 1994), with the following important distinction. The earlier model required specification of the mean velocity field in order to derive Reynolds stress (as the product of eddy viscosity and vertical shear). Thus, e.g., modeling the evolution of temperature and salinity in the OBL required solving time-dependent equations for both components of horizontal velocity in addition to conservation equations for heat and salt. The hypothesis underlying the present approach is that boundary layer turbulence responds primarily to surface forcing (stress and buoyancy flux) and adjusts rapidly (i.e., instantaneously) to any changes. Obviously, there will be times when this approximation is not valid: e.g., flows in which advection of turbulent kinetic energy by the mean flow is important. Nevertheless, this approach appears to have considerable merit, both for interpreting data taken in field conditions which are far from ideal, and as a candidate for an efficient numerical closure scheme.

2. Local turbulence closure

Closure is accomplished as follows. It is assumed that two length scales, λ_{max} and λ_{pyc}, describe the vertical influence of the energy containing turbulent eddies in the mixed layer and upper pycnocline, respectively. The former depends on surface friction velocity and surface buoyancy flux; the latter on friction velocity and buoyancy flux at the mixed layer/pycnocline interface. For neutrally or statically stable stratification, the mixing length in both cases follows a similarity theory described by McPhee (1981, 1994):

$$\lambda = \eta_*^2 \Lambda_* u_{*\lambda}/|f|, \tag{1}$$

where Λ_* is a similarity constant (0.028), R_c is the critical flux Richardson number (0.2), and:

$$\eta_* = \left(1 + \frac{\Lambda_* u_{*\lambda}}{\kappa |f| R_c L}\right)^{-1/2}, \tag{2}$$

is a stability factor that accounts for the tendency of stabilizing buoyancy flux to reduce the scale of

turbulence through the Obukhov length, $L = (u^3_{*\lambda})/(\kappa\langle w'b'\rangle_\lambda)$ where it is understood that the friction velocity and buoyancy flux refer to surface and pycnocline values in the respective layers, i.e.,

$$[u_{*\lambda},\langle w'b'\rangle_\lambda] = u_{*0},\langle w'b'\rangle_0 \quad z > z_{pyc},$$
$$[u_{*\lambda},\langle w'b'\rangle_\lambda] = u_{*pyc},\langle w'b'\rangle_{pyc} \quad z \le z_{pyc}, \qquad (3)$$

and $u_* = (\langle u'w'\rangle^2 + \langle v'w'\rangle^2)^{1/4}$ is friction velocity associated with local kinematic Reynolds stress. Note that in the neutral and stable limits, respectively,

$$\lambda_{max} \to \Lambda_* u_{*0}/|f| \quad L \to +\infty,$$
$$\lambda_{max} \to \kappa R_c L \quad L \to 0^+. \qquad (4)$$

For unstable buoyancy flux (or for near equatorial cases), the maximum mixing length is constrained by mixed layer depth: $\lambda_{max} \le \kappa|z_{pyc}|$ (for treatment of the statically unstable regime, refer the discussion of Fig. 15 of McPhee, 1994 and extensions suggested by McPhee, 1998). For shallow depths, a wall layer is introduced: $\lambda = \min(\kappa|z|, \lambda_{max})$; however, in a wave saturated environment, this may not be appropriate.

There are various ways to define the pycnocline elevation, z_{pyc}. Here, it is the level at which salinity (which controls density) exceeds its near surface value by 0.01 psu, but other approaches, such as a maximum buoyancy frequency cutoff, work as well. Although it might appear so, the mixing length model is not overly sensitive to the definition. The reason is that if slight stratification in what the eye would identify as the 'mixed layer' is enough to trigger the z_{pyc} criterion somewhere near the surface, L_{pyc} will still be relatively large and the geometric mean implicit in the stability factor (Eq. (2)) will retain a relatively large value for λ_{pyc}.

The velocity scale in the eddy viscosity relation is *local* friction velocity, hence,

$$K = u_* \lambda \qquad (5)$$

One could instead use $q = \sqrt{k}$ as the turbulent velocity scale, where k is twice the turbulent kinetic energy per unit mass, but since the idea here is to eliminate, e.g., solving a conservation equation for TKE, the Reynolds stress scale velocity is more straightforward. For regimes dominated by convection, a turbulent velocity scale based on surface buoyancy flux, w_*, is used in lieu of u_* (McPhee, 1998; Morison and McPhee, 1998); however, examples here are dominated by shear-driven turbulence.

In statically unstable or near neutral conditions, Reynolds analogy is assumed and eddy diffusivity is equal to eddy viscosity. In stably stratified flows, where momentum and scalar exchange may differ substantially, the ratio of eddy diffusivity to eddy viscosity is given by an approximation to the relation found by Turner (1973) for salt stratified flow in pipes;

$$\alpha(\mathrm{Ri}) = K_{H,S}/K = 1 \quad \mathrm{Ri} \le 0.79,$$
$$\alpha(\mathrm{Ri}) = K_{H,S}/K = e^{-1.5\sqrt{\mathrm{Ri}-0.79}} \quad 0.79 < \mathrm{Ri} < 5,$$
$$\alpha(\mathrm{Ri}) = K_{H,S}/K = 0.039 \quad \mathrm{Ri} \ge 5. \qquad (6)$$

where Ri is the gradient Richardson number.

The primary departure of LTC from other turbulence closure schemes comes in assuming that turbulent stress adjusts to surface forcing conditions rapidly, so that a 'steady state' solution of the momentum equation provides a good approximation to the instantaneous velocity and shear fields. At the outset, the distribution of u_* through the frictional boundary layer is unknown, thus, an iterative technique is used. The procedure is composed of the following steps.

(i) Calculate the maximum mixing length based on surface fluxes.

(ii) Use the analytic solution of Ekman stress equation (McPhee and Martinson, 1994) as a 'first guess' estimate of the friction velocity profile:

$$u_* = u_{*0} e^{\sqrt{|f|/(2u_{*0}\lambda)}(z/2)}. \qquad (7)$$

(iii) Calculate buoyancy flux and Richardson number for new estimates of eddy viscosity and diffusivity, then numerically solve the steady momentum equation again to obtain a new u_* profile.

(iv) Repeat (iii) until the change in eddy viscosity near the pycnocline is small.

In practice, this occurs after three or four repetitions. Although the method involves iteration (which is computationally expensive), it has several advantages over more conventional techniques. It provides a context for interpreting boundary layer measurements for which there exists no unambiguous recent history (e.g., in a regime with advection). It obviates the need for carrying prognostic equations for two components of velocity and additional prognostic equations for TKE and 'TKE moment' (MY $2\frac{1}{2}$) or

TKE and TKE dissipation ($k-\varepsilon$). Thus, e.g., the time evolution of the upper ocean T/S may be estimated with comparatively long time steps.

3. Data analysis and interpretation

Measurements from the 1994 Antarctic Zone Flux Experiment (ANZFLUX, see McPhee et al., 1996) provide an example of using LTC for describing turbulent fluxes in the entire OBL by combining turbulence measurements from one level with mean temperature and salinity profiles. The 2.4-h time period described here comes from a very active period as the ice station drifted over a warm core eddy during an intense storm. As the station advected onto the eddy, large changes in the OBL were observed, including shoaling of the pycnocline by about 100 m in 6 h. The situation was, thus, a severe test of the equilibrium assumption in the LTC approach.

An inverted mast with three *turbulence instrument clusters* (TICs) was deployed in the upper part of the boundary layer under ice about half a meter thick. Each TIC measured three orthogonal components of velocity, plus temperature, at scales small enough to be within the turbulent velocity and thermal inertial subranges (McPhee, 1992, 1994) as well as conductivity for mean salinity. A second mast, with two working TICs, was deployed deeper in the pycnocline. High-resolution profiles of upper ocean temperature and salinity were provided by a loose-tethered microstructure profiler (LMP) which continuously cycled at approximately 15 min intervals (T. Stanton, 1996, personal communication).

Both TIC and LMP temperature and conductivity sensors were independently calibrated against the project Sea-Bird Electronics 911 + yo − yo CTD. Average values in the upper 60 m are shown in Fig. 1, for a 2.4-h period centered at time 206.35 (UT, where 206 is the year day of 1994). This was during the drift onto the warm core eddy, while the pycnocline was shoaling rapidly. There was no sharp interface between a 'mixed layer' and the pycnocline. Indeed, the increasing slope with greater depth indicated intense mixing.

The model described in Section 2 requires friction velocity and buoyancy flux at the ice/ocean interface. The former was estimated by extrapolating u_* measured at the topmost TIC assuming an exponential decrease with depth. Heat flux at the interface was then calculated from $\langle w'T' \rangle_0 = c_H u_{*0} \delta T$ where δT is the temperature elevation of the mixed layer above freezing (obtained from T and S at the topmost TIC) and c_H is a heat transfer coefficient, approximately 0.006 (McPhee, 1992; McPhee et al., 1998). Measured heat flux was *not* used, because large gradients in turbulent heat flux were often observed during times of high heat flux. Using thermistors embedded in the ice, conductive heat flux was estimated to be about 30 W m^{-2}, and the difference between it and the oceanic heat flux provides the melt rate, which sets the buoyancy flux. With u_{*0} and $\langle w'b' \rangle_0$, and the observed T and S profiles, the model was solved and the modeled value of u_* at the topmost cluster was compared with observed. If it differed appreciably, u_{*0} was adjusted accordingly and the procedure repeated until the difference fell below a specified tolerance. Resulting friction velocity (stress) calculations are shown in Fig. 2A. The circle indicates that the model is forced to match u_* at the topmost cluster (about 3.4 m beneath the ice); however, the other measurements are independent. Stress at the interface exceeds 0.5 Pa.

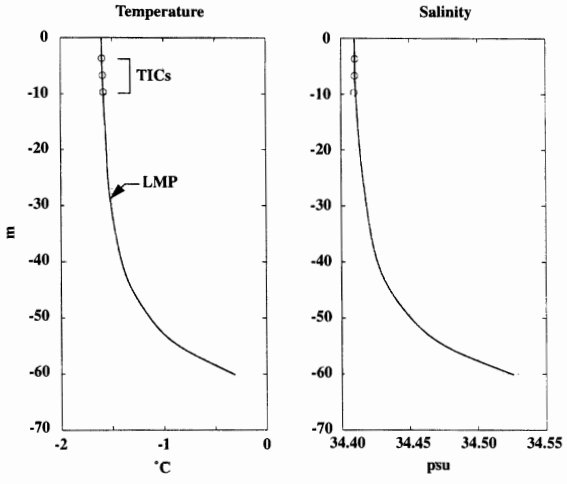

Fig. 1. Temperature and salinity structure of the upper ocean averaged for 2.4 h centered at time 206.35 UT, with three TICs operational in the upper part of the boundary layer. Profiles are from averages of LMP profiles taken at approximately 15-min intervals (LMP data courtesy of T. Stanton).

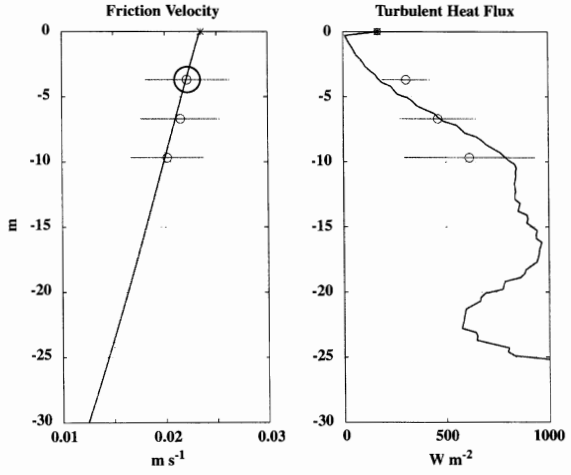

Fig. 2. (A) Modeled (solid curve) and observed (symbols with error bars) friction velocity (square root of the kinematic Reynolds stress) in the upper 30 m. (B) Modeled and observed turbulent heat flux. Observations comprise 2.4-h averages of 15-min realizations of the zero-lag covariance statistics, with error bars representing ± 1 standard deviation.

Since the model calculates eddy heat diffusivity, modeled heat flux may be obtained from the observed temperature profile. Results are compared to observations in Fig. 2B, and show exceptionally large values for an ice-covered ocean—similar values have been encountered only when ice had drifted into warm water in the marginal ice zone (McPhee, 1994). Obviously, a great deal of heat was being mixed upward as the ice moved rapidly over the warm eddy. The decrease in modeled heat flux near the surface is an artifact of forcing the temperature gradient to zero near the top of the LMP sampling range.

It is worth noting that Reynolds stress is constrained to fall from the surface value to relatively small values somewhere near the top of the pycnocline, thus, a fairly wide range of eddy viscosity (K_M) will give similar solutions for u_*. No similar constraint exists for heat flux. Given the observed temperature gradient, one needs a realistic distribution of eddy diffusivity (K_H) to get the heat flux right. Consequently, the model-observation comparison between both momentum and heat flux in Fig. 2 is particularly important. Several other examples comparing modeled and observed fluxes were calculated, with generally similar results. One for which surface stress was much less and stratification in the upper part of the boundary layer was stronger is described by McPhee et al. (1998).

Table 1
Comparison listing features of the two boundary layer models used to simulate the idealized Weddell Sea storm scenario

Local turbulence closure model	Mellor–Yamada Level $2\frac{1}{2}$ model
Prognostic equations	
$T_t = (\alpha K T_z)_z$	$T_t = (K_H T_z)_z$
$S_t = (\alpha K S_z)_z$	$S_t = (K_H S_z)_z$
	$\hat{u}_t + if_{cor}\hat{u} = (K_M \hat{u}_z)_z$ [two equations]
	$q_t^2 = (K_Q q_z^2)_z + P_S + P_B - \varepsilon$
	$(q^2 l)_t = (K_Q (q^2 l)_z)_z + lE_1(P_S + P_B) - (q^3/l)\{1 + E_2(l/\kappa L)^2\}$
Turbulence closure	
$K = u_* \lambda$	$l = q^2 l / q^2$
$\alpha = \alpha(\mathrm{Ri})$	$K_Q = S_Q q l$
	$K_M = S_M q l$
	$K_H = S_H q l$
Timestep: 6 h	Timestep: 1 h

The model domain for each is the upper 150 m of the ocean, with approximately 3 m resolution in the vertical. Subscripts z and t denote differentiation with respect to vertical displacement and time, respectively.
K is determined for each timestep from *local conditions* of surface stress and buoyancy flux with the current T/S profiles as described in the text. Conservation equations are solved implicitly with a leap-frog scheme using staggered grids.
S_Q is constant; S_M and S_H are stability parameters dependent on the local nondimensional shear and buoyancy flux. Conservation equations are solved implicitly with a leap-frog scheme using staggered grids.

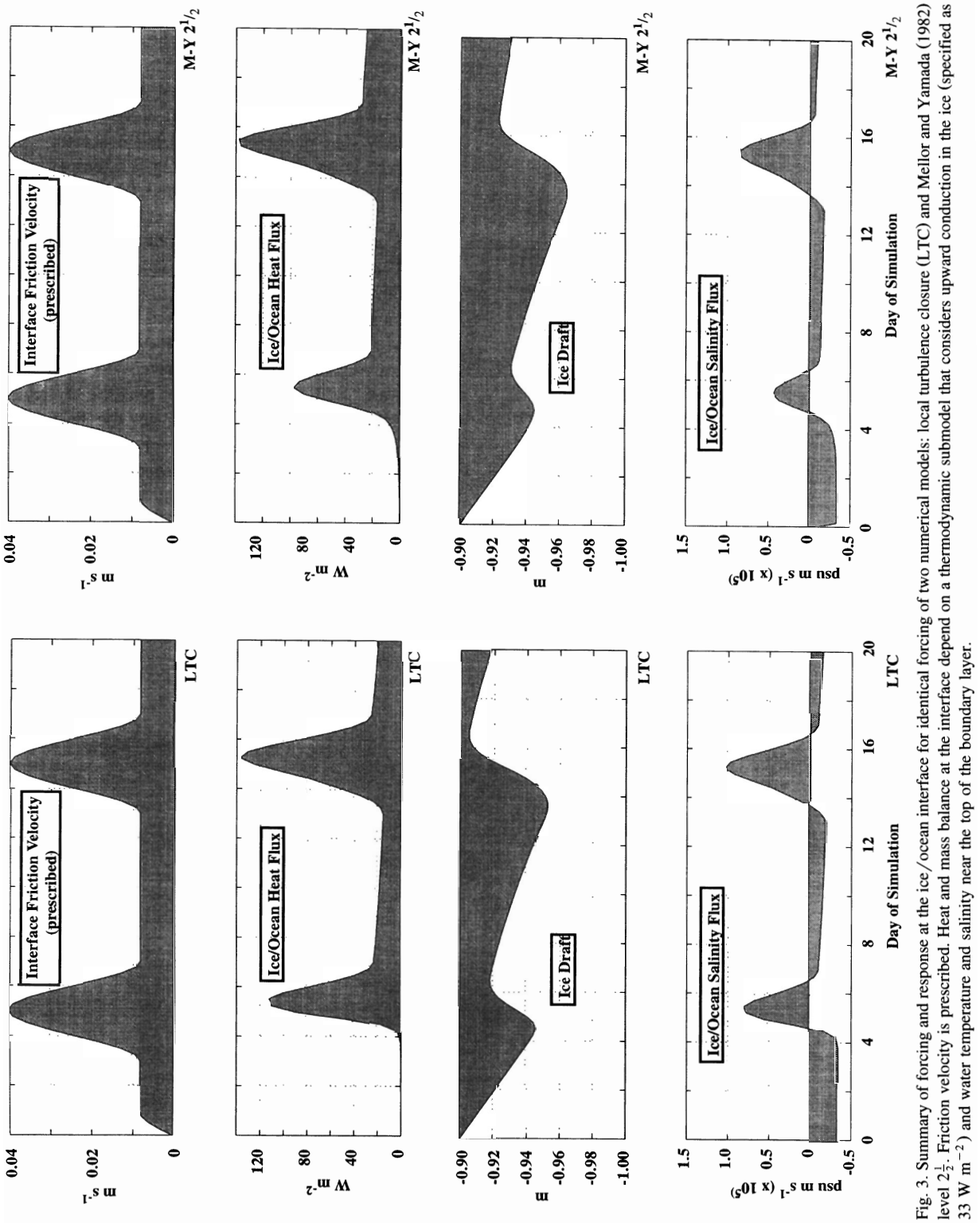

Fig. 3. Summary of forcing and response at the ice/ocean interface for identical forcing of two numerical models: local turbulence closure (LTC) and Mellor and Yamada (1982) level $2\frac{1}{2}$. Friction velocity is prescribed. Heat and mass balance at the interface depend on a thermodynamic submodel that considers upward conduction in the ice (specified as 33 W m^{-2}) and water temperature and salinity near the top of the boundary layer.

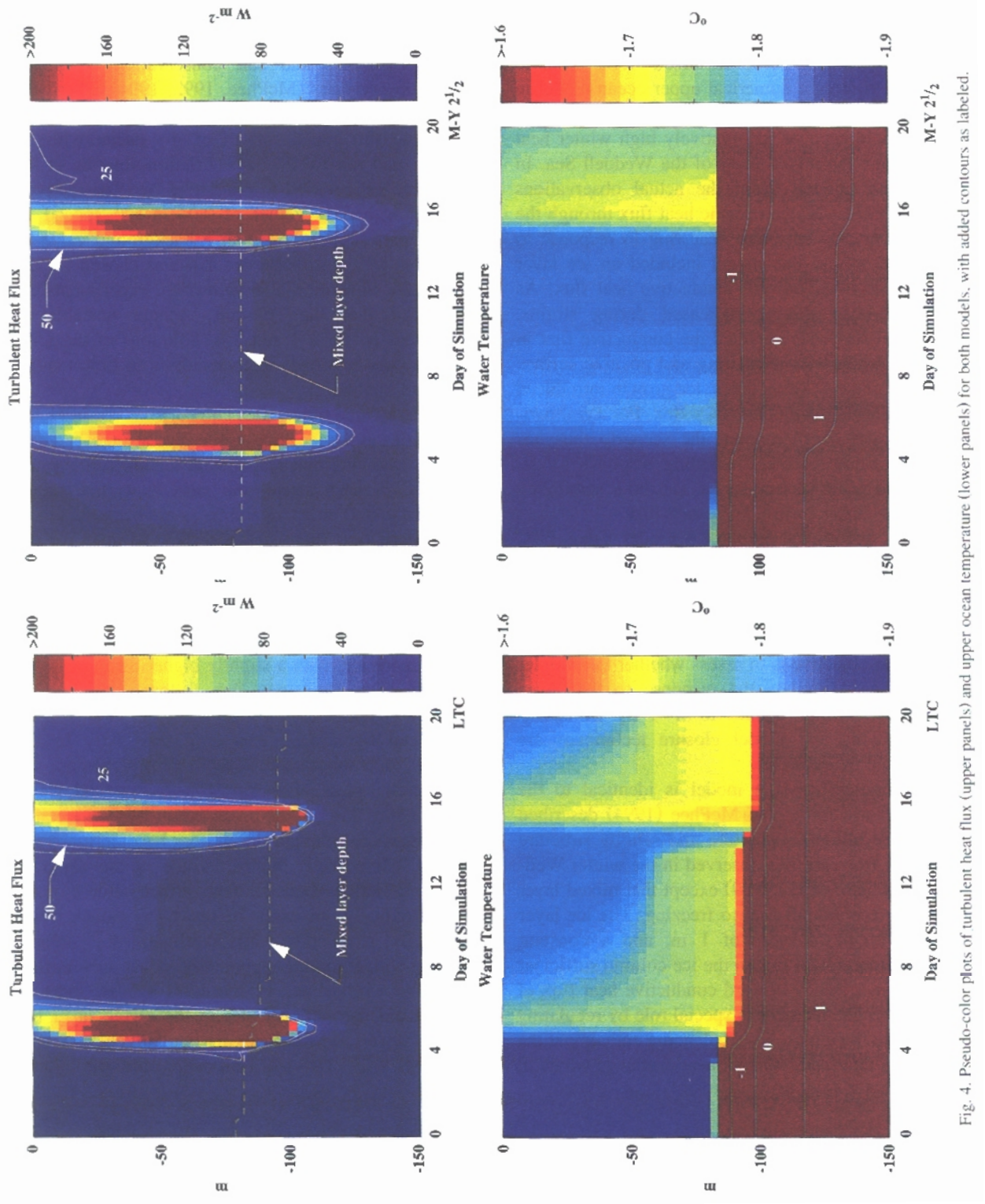

Fig. 4. Pseudo-color plots of turbulent heat flux (upper panels) and upper ocean temperature (lower panels) for both models, with added contours as labeled.

4. Prognostic modeling

In McPhee (1994), an idealized storm scenario was used to force a numerical upper ocean model in order to illustrate how nonlinear stirring from intense storms could account for relatively high winter heat flux through the mixed layer of the Weddell Sea. In the original model, as in the actual observations during ANZFLUX, the oceanic heat flux through the mixed layer was episodic, occurring in response to gale force winds. The model included an ice layer with a prescribed upward conductive heat flux. As boundary layer mixing increased during storms, ocean heat flux overwhelmed the conductive flux in the ice causing bottom melting and positive surface buoyancy flux. At other times, ice growth introduced statically destabilizing buoyancy flux. For a comparison of upper ocean models, the scenario thus has many desirable features, including response to extreme (full gale) surface stress, and both stabilizing and destabilizing surface buoyancy flux.

In this section, a prognostic model using LTC closure with time- dependent conservations equations for temperature and salinity only, is compared to a realistic and widely used second-moment closure model: M–Y level $2\frac{1}{2}$ (Mellor and Yamada, 1982). The objective is to assess whether the simpler approach can simulate the response to the storm scenario in a similar manner to M–Y $2\frac{1}{2}$. Conservation equations and model closure techniques are summarized in Table 1.

The forcing for each model is identical to the storm scenario forcing of McPhee (1994) described above. The initial temperature and salinity structure was taken from profiles observed in the winter Weddell Sea (Huber et al., 1989) except that mixed layer temperature is initially set to freezing. The ice layer begins with a thickness of 1 m, and a constant temperature gradient within the ice column sufficient to maintain a steady upward conductive heat flux of 33 W m^{-2}. The ice plays a special role by regulating heat loss to the atmosphere, balancing enthalpy at the ice/ocean interface by latent heat exchange which in turn provides salinity (buoyancy) flux. The process is incorporated in each model using a submodel of thermodynamics and salt conservation developed from observations (McPhee, 1992, 1994). The models were implemented on identical staggered grids covering the upper 150 m of the ocean with 50 levels, and ran for 20 days. Friction velocity at the interface is specified to consist of two 'cosine-bell' storms with peak values of 0.04 m s^{-1} spaced 10 days apart superimposed on a background value of 0.008 m s^{-1}. A timestep of 1 h was chosen for the M–Y $2\frac{1}{2}$ simulation after numerical experiments established that the solution became unstable at timesteps between 1 and 2 h. Solutions of the LTC model were relatively unchanged out to timesteps of 6 h and beyond.

Side-by-side time-series comparisons of simulated properties at the ice/ocean interface are presented in Fig. 3, showing that response at the surface is quite similar. In each storm, the peak heat flux values (second panel) are comparable, as are mean values of ice/ocean heat flux: 30.8 and 28.9 W m^{-2} for the LTC and M–Y $2\frac{1}{2}$ models, respectively. Similar patterns of slow ice growth between storms with rapid ablation during the large heat flux events are predicted, although the M–Y $2\frac{1}{2}$ model grows about 1 cm more ice, with a slightly higher mean negative salinity flux. Buoyancy flux follows salinity flux closely at temperatures near freezing, so mixing is enhanced by surface buoyancy flux early in the storms, then suppressed as rapid melting begins.

Contour plots of turbulent heat flux and water temperature through the upper ocean (Fig. 4) are also quite similar, although differences become more apparent. Mixed-layer depth, defined as the depth at which salinity exceeds its near surface value by 0.01 psu, gradually increases in the LTC model. With M–Y $2\frac{1}{2}$, it remains nearly constant, which is surprising since mixing apparently penetrates farther into the pycnocline. In the LTC model, there is significant thermal structure in the mixed layer between storms, whereas mixing is relatively complete with M–Y $2\frac{1}{2}$. Delving a bit deeper into the models

Fig. 5. Shaded contour plots of K_H (upper panels) for both models (in the LTC model, $K_H = \alpha K$) and turbulent length scale (lower panels). Note that λ and l have different meaning as described in the text, but that they should be comparable where the water column is well-mixed in density, generally above the mixed layer depth of Fig. 4.

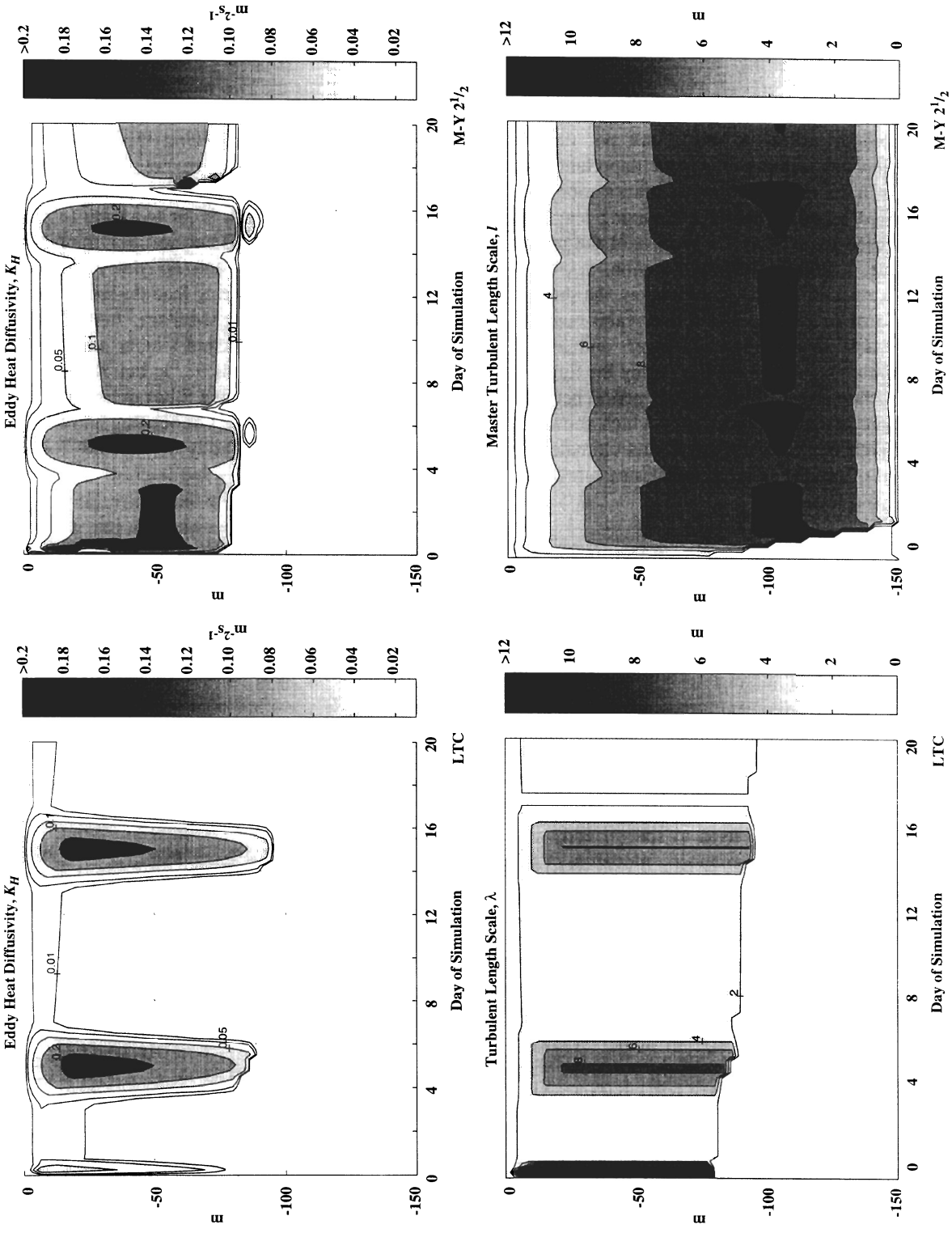
Eddy Heat Diffusivity, K_H
Master Turbulent Length Scale, l
Turbulent Length Scale, λ
Day of Simulation
M-Y $2^1/_2$
LTC
m
m^2s^{-1}
>0.2
0.18
0.16
0.14
0.12
0.10
0.08
0.06
0.04
0.02
>12
10
8
6
4
2
0
-50
-100
-150
0
4
8
12
16
20
0.01
0.05
0.1
0.2
1.2

(Fig. 5) indicates why between the storms (days 8 to 12), mixed layer eddy heat diffusivity (upper panels) in the M–Y $2\frac{1}{2}$ is nearly an order of magnitude greater than the LTC model. Part of the reason for this is illustrated in the lower panels. Despite the fact that the length scales, λ and l, are not directly comparable when stability effects are important, they are similar in the absence of much stratification (i.e., in the mixed layer). In M–Y $2\frac{1}{2}$, mixing length in the sense used for LTC is the product of the master length scale, l, times a stability function, S_H, times the ratio q/u_*. In neutral stratification, the product $S_H q/u_*$ is of order one, so the two scales ought to be comparable in a well-mixed layer, and indeed their maximum values are similar during the times of extreme surface stress. In the calmer period between storms, there is a large discrepancy which shows up as the difference in eddy diffusivity and ultimately in the amount of mixing of temperature structure in the density mixed layer.

5. Discussion

The LTC model provides a relatively simple method for estimating flux of momentum and scalar variables in the OBL. It retains important observed features of turbulent mixing, and in that sense, is more akin to second-moment turbulence closure than to bulk property mixed layer models. It provides a useful tool for interpreting and extrapolating measurements in the OBL, as demonstrated in Section 3 and elsewhere (McPhee et al., 1998).

The LTC may also be used to specify eddy viscosity and diffusivity for prognostic modeling of the evolution of temperature and density structure in the upper ocean. Section 4 demonstrated performance comparable to a sophisticated second-moment closure model, but with a much longer timestep and carrying only two prognostic conservation equations instead of six. Solutions were obtained for each model forced by a relatively 'difficult' modeling scenario. Many characteristics of the solutions were quite similar, including heat flux at the surface which is indicative of the amount of heat entrained from below the mixed layer. On a more esoteric plane, there were some important differences (e.g., an order of magnitude disparity in eddy diffusivity between storms, Fig. 5) and it is germane to ask whether there is any way of discriminating between the models at this level.

During the period between simulated storms, surface conditions for the two models are similar. Friction velocity is specified at 0.008 m s^{-1} and buoyancy flux dependent on freezing is about -1.3×10^{-8} W kg^{-1}. This is relatively mild buoyancy production of TKE and implies an Obukhov length of around -100 m, which is far too large to play a controlling role in the TKE balance. For comparison, consider Reynolds stress and buoyancy flux measured at the edge of a freezing lead during the Arctic Leads Experiment in 1992 (McPhee, 1994; McPhee and Stanton, 1996). We found similar stress conditions there ($u_* = 0.007$ m s^{-1}), but destabilizing buoyancy flux was about five times greater (because ice growth was much faster), producing an Obukhov length of about -12 m. Eddy diffusivities for heat and salt were between 0.04 and 0.05 m^2 s^{-1}, which is much larger than they would have been under neutrally stratified surface conditions, but still much less than the M–Y $2\frac{1}{2}$ model predictions of Section 4, where there was considerably less TKE production by buoyancy. The data thus suggest that the mixing length produced by the second-moment model was too large. The example also demonstrates that under certain conditions, it is feasible to test ocean turbulence models in ways not often used before.

Acknowledgements

I am indebted to T. Stanton for providing the LMP profile data. Funding support provided by the National Science Foundation through grant OPP 9410848 and the Office of Naval Research, through contracts N00014-94-C-0023 and N00014-96-C-0032, is gratefully acknowledged.

References

Burchard, H., Baumert, H., 1995. On the performance of a mixed layer model based on the $k-\varepsilon$ turbulence closure. J. Geophys. Res. 100, 8523–8540.

Businger, J.A., Wyngaard, J.C., Izumi, Y., Bradley, E.F., 1971. Flux–profile relationships in the atmospheric surface layer. J. Atmos. Sci. 28, 181–189.

Huber, B.A., Mele, P.A., Haines, W.E., Gordon, A.L., Jennings, J.C., Gordon, L.I., Weiss, R.F., Van Woy, F.A., Salaneh, P.K.,

1989. CTD and hydrographic data from Cruise ANT V/2 of R/V *Polarstern*. Tech. Rep. LDGO-89-3, 245 pp. [Available from Lamont-Doherty Earth Observatory, Palisades, NY 10964, USA].

McPhee, M.G., 1981. An analytic similarity theory for the planetary boundary layer stabilized by surface buoyancy. Boundary-Layer Meteorol. 21, 325–339.

McPhee, M.G., 1992. Turbulent heat flux in the upper ocean under sea ice. J. Geophys. Res. 97, 5365–5379.

McPhee, M.G., 1994. On the turbulent mixing length in the oceanic boundary layer. J. Phys. Oceanogr. 24, 2014–2031.

McPhee, M.G., 1998. An inertial-dissipation method for estimating turbulent flux in buoyancy driven, convective boundary layers. J. Geophys. Res. 103, 3249–3255.

McPhee, M.G., Martinson, D.G., 1994. Turbulent mixing under drifting pack ice in the Weddell Sea. Science 263, 218–221.

McPhee, M.G., Stanton, T.P., 1996. Turbulence in the statically unstable oceanic boundary layer under Arctic leads. J. Geophys. Res. 101, 6409–6428.

McPhee, M.G., Ackley, S.F., Guest, P., Huber, B.A., Martinson, D.G., Morison, J.H., Muench, R.D., Padman, L., Stanton, T.P., 1996. The Antarctic Zone Flux Experiment. Bull. Am. Met. Soc. 77, 1221–1232.

McPhee, M.G., Kottmeier, C., Morison, J.M., 1998. Ocean heat flux in the central Weddell Sea during winter, J. Phys. Oceanogr., in press.

Mellor, G.L., Yamada, T., 1982. Development of a turbulence closure model for geophysical fluid problems. Rev. Geophys. 20, 851–875.

Morison, J.M., McPhee, M.G., 1998. The horizontal structure of lead convection measured with an autonomous vehicle. J. Geophys. Res. 103, 3257–3281.

Price, J.F., Weller, R.A., Pinkel, R., 1986. Diurnal cycling: observations and models of the upper ocean response to diurnal heating, cooling, and wind mixing. J. Geophys. Res. 91, 8411–8427.

Turner, J.S., 1973. Buoyancy Effects in Fluids. Cambridge Univ. Press, London, 367 pp.